
Observable Neural ODEs for Identifiable Causal Forecasting in Continuous Time

Jennifer Wendland
wendland@uni-koblenz.de

Nicolas Freitag
nfreitag@uni-koblenz.de

Maik Kschischo
kschischo@uni-koblenz.de
Department of Computer Science
University of Koblenz
53424 Koblenz, Germany

Abstract

Causal inference in continuous-time sequential decision problems is challenged by hidden confounders. We show that, in latent state-space models with time-varying interventions, observability of the latent dynamics from observed data is necessary for identifying dynamic treatment effects, linking control-theoretic observability to causal identifiability, even when hidden confounders affect both treatments and outcomes.

We derive a continuous-time adjustment formula expressing potential outcome distributions under treatment trajectories via the measurement model, latent dynamics, and the filtering distribution over latent states given observed histories.

We propose Observable Neural ODEs (ObsNODEs), Neural ODE models in observable normal form for causal forecasting. ObsNODEs learn continuous-time dynamics with states reconstructible from observations, enabling outcome prediction under alternative treatment paths.

Experiments on synthetic cancer data, semi-synthetic data based on MIMIC-IV, and real-world sepsis data show strong performance over recent sequence models.

1 Introduction

Sequential decision-making requires predicting how actions affect future outcomes under evolving observations. In medicine, this arises in dynamic treatment regimes (DTRs), where treatments are repeatedly adapted to a patient’s longitudinal history (Murphy, 2003; Robins, 2004).

A central challenge is the identifiability of causal treatment effects in continuous time. In observational data, time-dependent confounding and treatment-confounder feedback arise when covariates affect both treatment assignment and outcomes while being themselves affected by earlier treatments (Hernán, Robins, 2023). Hidden confounders further complicate this problem, since the relevant disease state is only partially observed.

We address this problem from a state-space perspective. We introduce *ObsNODEs*, a class of Neural ODE models in observable normal form, and show that observability of the latent state is a necessary condition for identifying dynamic treatment effects in latent continuous-time systems with hidden confounding. This establishes a link between the control-theoretic notion of observability and causal identifiability in continuous-time treatment models. Based on this insight, ObsNODEs support causal forecasting under discrete and continuous treatment trajectories.

Contributions. (i) We show that observability of the latent state is necessary for identifiability of dynamic treatment effects in latent continuous-time state-space models with hidden confounding affecting both treatment and outcomes, and derive a corresponding continuous-time causal adjustment formula. (ii) We propose *ObsNODEs*, Neural ODE models in observable normal form that enforce observability by construction for causal forecasting under dynamic treatment regimes. (iii) We evaluate ObsNODEs on synthetic cancer data, semi-synthetic MIMIC-IV data, and a real-world sepsis example, demonstrating strong causal forecasting performance compared to recent sequence models.

2 Problem statement

We assume to observe a continuous-time multivariate outcome process \mathbf{Y}_t and a time-varying treatment process \mathbf{A}_t for times $t \in [0, t_c]$. Given the history $\{\mathbf{a}_{[0, t_c]}, \mathbf{y}_{[0, t_c]}\}$ with $\mathbf{a}_{[0, t_c]} = \{\mathbf{A}_t = \mathbf{a}_t | 0 \leq t < t_c\}$ and $\mathbf{y}_{[0, t_c]} = \{\mathbf{Y}_t = \mathbf{y}_t | 0 \leq t \leq t_c\}$, the goal is to predict the probability density of the conditional potential outcome $\mathbf{Y}_t(\mathbf{a}_{[t_c, t_c+s]})$ on $[t_c, t_c + s)$ under a hypothetical treatment path $\mathbf{a}_{[t_c, t_c+s]} = \{\mathbf{A}_t = \mathbf{a}_t | t_c \leq t < t_c + s\}$.

In clinical applications, \mathbf{Y}_t may contain irregularly sampled laboratory values, vital signs, or imaging embeddings, while \mathbf{A}_t represents binary, categorical, or continuous treatments. Outside randomized trials, treatment assignment depends on the evolving patient history, which induces time-dependent confounding and treatment-confounder feedback.

We treat all measured variables as components of \mathbf{Y}_t and define outcomes, when needed, as functions of \mathbf{Y}_t . This entails no loss of generality for the identification results below. We use outcome and observed process interchangeably for \mathbf{Y}_t .

3 Preliminaries

3.1 Nonlinear state-space model

A continuous-time deterministic state-space model is given by

$$\dot{\mathbf{z}}_t = \mathbf{f}(\mathbf{z}_t, \mathbf{a}_t), \quad (1a)$$

$$\mathbf{y}_t = \mathbf{h}(\mathbf{z}_t), \quad (1b)$$

$$\mathbf{z}_0 = \boldsymbol{\zeta}, \quad (1c)$$

where $\mathbf{z}_t \in \mathbb{R}^{d_z}$ is a latent state, $\mathbf{a}_t \in \mathbb{R}^{d_a}$ a treatment or control, and $\mathbf{y}_t \in \mathbb{R}^{d_y}$ the observed process. The measurement function \mathbf{h} is not necessarily invertible, in particular when $d_z > d_y$. We assume \mathbf{f} is Lipschitz in \mathbf{z} , so the system admits a unique solution for any admissible control path and initial condition.

For a given control path, observability asks whether the latent state or, equivalently, its initial value, is uniquely determined by the observed output over a finite horizon (Bernard, 2019). For a given control \mathbf{a} and initial condition $\mathbf{z}_0 = \boldsymbol{\zeta}$, let $\mathbf{z}_t(\mathbf{a}, \boldsymbol{\zeta})$ denote the resulting state trajectory, and define the corresponding output trajectory by $\mathbf{y}_t(\mathbf{a}, \boldsymbol{\zeta}) := \mathbf{h}(\mathbf{z}_t(\mathbf{a}, \boldsymbol{\zeta}))$.

Definition 3.1. The system (1) is **uniformly observable** on an open set $U \subset \mathbb{R}^{d_z}$ if, for any control path $\mathbf{a} : [0, T] \rightarrow \mathbb{R}^{d_a}$ and any $\boldsymbol{\zeta}, \boldsymbol{\eta} \in U$,

$$\mathbf{y}_t(\mathbf{a}, \boldsymbol{\zeta}) = \mathbf{y}_t(\mathbf{a}, \boldsymbol{\eta}) \quad \forall t \in [0, T] \implies \boldsymbol{\zeta} = \boldsymbol{\eta},$$

where $[0, T]$ is the maximal interval on which both solutions exist.

3.2 Potential outcomes and graphical causal models

We use the potential-outcomes framework and graphical causal models to formalize interventions (Robins, 1986; Pearl, 2000; Peters et al., 2017; Hernán, Robins, 2023). For a treatment path $\mathbf{a}_{[0, T]}$, let $\mathbf{Y}_t(\mathbf{a}_{[0, t]})$ denote the potential outcome process. We assume consistency and the stable unit treatment value assumption (SUTVA), which excludes that the potential outcome of one unit is affected by treatments of other units and that there are no different forms or versions of a treatment (Rubin, 1980; Hernán, Robins, 2023). In longitudinal observational settings, identifiability is complicated by time-dependent confounding and treatment-confounder feedback.

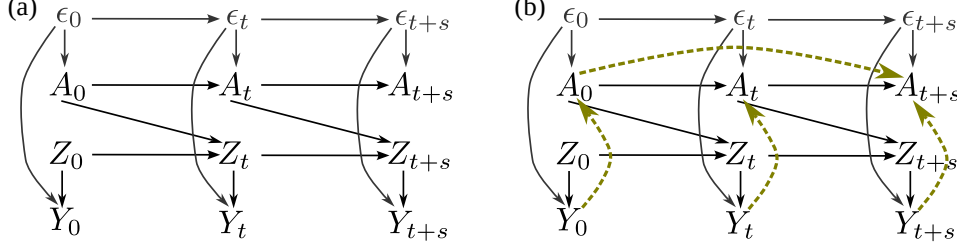


Figure 1: (a) Temporal DAG for treatment A , outcome Y , and latent state Z at three consecutive time points $0, t$ and $t + s$. The process ϵ_t is a hidden confounder affecting both treatment and outcome. (b) In a dynamic treatment regime, treatment depends on treatment and outcome history, as indicated by green dashed arrows.

3.2.1 The conditional front-door criterion

To connect causal identification with latent state-space models, we use the conditional front-door criterion (Xu et al., 2024), an extension of the front-door criterion (Pearl, 2000) for estimating the effect of an intervention in the presence of an unobserved common cause of both treatment and outcome:

Theorem 3.2. (Xu et al., 2024) *A set of variables M fulfills the **conditional front-door criterion (CFD)** relative to the ordered pair of variables (A, Y) in a directed acyclic graph (DAG) \mathcal{G} , if (i) M intercepts all directed paths from A to Y , (ii) there exists a set of conditioning variables W that blocks all backdoor paths from A to M and (iii) all backdoor path between M and Y are blocked by $\{A\} \cup W$. If M fulfills the CFD relative to (A, Y) with conditioning variables W the causal effect estimate is given by*

$$P(Y(a)) = \sum_{m, w, a'} P(y|a', m, w)P(a'|w)P(m|a, w)P(w), \quad (2)$$

where the sum over a' runs over alternative treatments.

4 Observable Neural ODEs for dynamic treatment regimes

We model the observed process by a latent Neural ODE (Chen et al., 2018; Rubanova et al., 2019; Kidger et al., 2020) with parameters θ

$$\mathbf{Z}_0 \sim p_\theta(\mathbf{Z}_0), \quad \dot{\mathbf{Z}}_t = \mathbf{f}_\theta(\mathbf{Z}_t, \mathbf{A}_t), \quad \mathbf{Y}_t \sim q_\theta(\cdot | \mathbf{Z}_t, \epsilon_t), \quad (3)$$

where p_θ parameterizes the initial state distribution, \mathbf{f}_θ the vector field, and q_θ the observation model. We interpret the treatment process as an intervention on the latent dynamics, as illustrated in Fig. 1(a). Typically, the treatment is adjusted according to the observations and we have a dynamic treatment regime (Murphy, 2003; Robins, 2004; Hernán, Robins, 2023): $\mathbf{A}_t = \boldsymbol{\pi}(\mathbf{y}_t, \mathbf{y}_{[0,t]}, \mathbf{a}_{[0,t]})$ (see Fig. 1(b)). An unobserved process ϵ_t that influences both the outcome and treatment acts as a hidden time-dependent confounder, and the treatment policy $\boldsymbol{\pi}$ may therefore also depend on ϵ_t .

4.1 Causal identifiability for the state-space model with hidden confounding

Given observed history $\mathbf{o}_{[0,t]} = \{\mathbf{a}_{[0,t]}, \mathbf{y}_{[0,t]}\}$ and current observation $\mathbf{Y}_t = \mathbf{y}_t$, we seek the conditional density of the potential outcome at time $t + s$ under a hypothetical future treatment path $\mathbf{a}_{[t,t+s]}$. Under consistency, SUTVA, and an observable latent state-space model of the form (3), this density is identified by

$$\begin{aligned} & P_{\mathbf{Y}_{t+s}(\mathbf{a}_{[t,t+s]}) | \mathbf{Y}_t, \mathbf{o}_{[0,t]}}(\mathbf{y}_{t+s} | \mathbf{y}_t, \mathbf{o}_{[0,t]}) \\ &= \int_{\mathbf{z}_{t+s}} \int_{\mathbf{z}_t} p(\mathbf{z}_t | \mathbf{y}_t, \mathbf{o}_{[0,t]}) p(\mathbf{z}_{t+s} | \mathbf{a}_{[t,t+s]}, \mathbf{z}_t) p(\mathbf{y}_{t+s} | \mathbf{z}_{t+s}), \end{aligned} \quad (4)$$

even if there is time dependent confounding by an unobserved dynamic process ϵ_t affecting both treatment \mathbf{A}_t and outcome \mathbf{Y}_t (see Fig. 1).

The key requirement is that the latent state is observable from the observed history; otherwise the filtering density $p(\mathbf{z}_t | \mathbf{y}_t, \mathbf{o}_{[0,t]})$ remains spread over states that explain the treatment-observation history equally well, preventing identification of causal effects. For the deterministic ODE in (3) the dynamics is given by the point mass: $p(\mathbf{z}_{t+s} | \mathbf{a}_{[t,t+s]}, \mathbf{z}_t) = \delta(\mathbf{z}_{t+s} - \mathbf{z}_t - \int_t^{t+s} \mathbf{f}(\mathbf{z}_\tau, \mathbf{a}_\tau) d\tau)$. The adjustment formula (4) also applies to dynamic treatment regimes (Figure 1(b)), where the current observation and observed history $\mathbf{y}_t, \mathbf{o}_{[0,t]}$ is used to guide the future treatment path $\mathbf{a}_{[t,t+s]}$.

4.1.1 Derivation of a discrete time version of equation (4) from the CFD

We derive a time discretized version of (4) and relegate details for the continuous time version to appendix A.1. Consider three consecutive time points 0, t and $t+s$. A time-discretized approximation of the ODE in (3) is given by $\mathbf{Z}_{t+s} \approx \mathbf{Z}_t + \mathbf{f}(\mathbf{z}_t, \mathbf{a}_t) s$. Assume we have observed $\mathbf{o}_0 = \{\mathbf{a}_0, \mathbf{y}_0\}$ and \mathbf{y}_t . To apply the CFD in theorem 3.2 we make the following identifications

$$A \leftarrow \mathbf{A}_t, \quad Y \leftarrow \mathbf{Y}_{t+s}, \quad M \leftarrow \mathbf{Z}_{t+s}, \quad W \leftarrow \{\mathbf{Z}_t, \mathbf{Y}_t, \mathbf{A}_0, \mathbf{Y}_0\} = \{\mathbf{Z}_t, \mathbf{Y}_t, \mathbf{O}_0\}.$$

Then, we can check graphically in Fig. 1(a,b) that $M = \mathbf{Z}_{t+s}$ fulfills the CFD-criterion relative to the ordered pair $(A, Y) = (\mathbf{A}_t, \mathbf{Y}_{t+s})$, if we use $W = \{\mathbf{Z}_t, \mathbf{Y}_t, \mathbf{O}_{[0,t]}\}$ as conditioning set. Now we compute the probability density for the potential outcome $Y_{t+s}(\mathbf{a}_t)$ when applying treatment $\mathbf{A}_t = \mathbf{a}_t$ at time t using (2) and replacing the sums by integrals

$$P_{Y_{t+s}(\mathbf{a}_t)}(\mathbf{y}_{t+s}) = \int_{\mathbf{z}_{t+s}} \int_{\mathbf{z}_t, \mathbf{y}_t, \mathbf{o}_0} \int_{\mathbf{a}'_t} \{p(\mathbf{y}_{t+s} | \mathbf{a}'_t, \mathbf{z}_{t+s}, \mathbf{z}_t, \mathbf{y}_t, \mathbf{o}_0) \cdot p(\mathbf{a}'_t | \mathbf{z}_t, \mathbf{y}_t, \mathbf{o}_0) p(\mathbf{z}_{t+s} | \mathbf{a}_t, \mathbf{z}_t, \mathbf{y}_t, \mathbf{o}_0) p(\mathbf{z}_t, \mathbf{y}_t, \mathbf{o}_0)\}.$$

For the model (3) we have the following independence relations

$$\begin{aligned} p(\mathbf{y}_{t+s} | \mathbf{a}'_t, \mathbf{z}_{t+s}, \mathbf{z}_t, \mathbf{y}_t, \mathbf{o}_0) &= p(\mathbf{y}_{t+s} | \mathbf{z}_{t+s}) \\ p(\mathbf{z}_{t+s} | \mathbf{a}_t, \mathbf{z}_t, \mathbf{y}_t, \mathbf{o}_0) &= p(\mathbf{z}_{t+s} | \mathbf{a}_t, \mathbf{z}_t). \end{aligned}$$

Integrating over \mathbf{a}'_t and using $p(\mathbf{z}_t, \mathbf{y}_t, \mathbf{o}_0) = p(\mathbf{z}_t | \mathbf{y}_t, \mathbf{o}_0) p(\mathbf{y}_t, \mathbf{o}_0)$ we find

$$P_{Y_{t+s}(\mathbf{a}_t)}(\mathbf{y}_{t+s}) = \int_{\mathbf{z}_{t+s}} \int_{\mathbf{z}_t, \mathbf{y}_t, \mathbf{o}_0} \{p(\mathbf{y}_{t+s} | \mathbf{z}_{t+s}) p(\mathbf{z}_{t+s} | \mathbf{a}_t, \mathbf{z}_t) p(\mathbf{z}_t | \mathbf{y}_t, \mathbf{o}_0) p(\mathbf{y}_t, \mathbf{o}_0)\},$$

from which we read the conditional density for the potential outcome $Y_{t+s}(\mathbf{a}_t)$ when applying treatment $\mathbf{A}_t = \mathbf{a}_t$ at time t , given we have observed outcome \mathbf{y}_t at time t and the treatment/outcome history \mathbf{o}_0 at time zero

$$P_{Y_{t+s}(\mathbf{a}_t) | \mathbf{Y}_t, \mathbf{O}_0}(\mathbf{y}_{t+s} | \mathbf{y}_t, \mathbf{o}_0) = \int_{\mathbf{z}_{t+s}} \int_{\mathbf{z}_t} \{p(\mathbf{y}_{t+s} | \mathbf{z}_{t+s}) p(\mathbf{z}_{t+s} | \mathbf{a}_t, \mathbf{z}_t) p(\mathbf{z}_t | \mathbf{y}_t, \mathbf{o}_0)\}.$$

4.2 Neural ODEs in observable normal form (ObsNODEs)

The identification formula (4) requires that the latent state can be inferred from observed outcomes and treatment history. Standard latent Neural ODEs do not guarantee this property. We therefore parameterize the latent dynamics in continuous triangular observable normal form (Bernard, 2019; Adamy, 2024):

$$\dot{\mathbf{Z}}_t = \begin{pmatrix} \dot{\mathbf{Z}}_t^{(1)} \\ \vdots \\ \dot{\mathbf{Z}}_t^{(i)} \\ \vdots \\ \dot{\mathbf{Z}}_t^{(m)} \end{pmatrix} = \begin{pmatrix} \mathbf{Z}_t^{(2)} + \phi_{\theta_1}^{(1)}(\mathbf{Z}_t^{(1)}, \mathbf{a}_t) \\ \vdots \\ \mathbf{Z}_t^{(i+1)} + \phi_{\theta_i}^{(i)}(\mathbf{Z}_t^{(1)}, \dots, \mathbf{Z}_t^{(i)}, \mathbf{a}_t) \\ \vdots \\ \phi_{\theta_m}^{(m)}(\mathbf{Z}_t, \mathbf{a}_t) \end{pmatrix}, \quad \mathbf{Y}_t = \mathbf{Z}_t^{(1)}. \quad (5)$$

Here the state $\mathbf{Z}_t = (\mathbf{Z}_t^{(1)}, \dots, \mathbf{Z}_t^{(m)}) \in \mathbb{R}^{d_z}$ is partitioned into m blocks $\mathbf{Z}_t^{(i)} \in \mathbb{R}^{d_y}$, so that $d_z = md_y$, and each $\phi_{\theta_i}^{(i)}$ is implemented by a neural network. Under fairly general conditions (Bernard, 2019), an observable system in the form (1) can be transformed into the observable normal form (5). In practice we allow additive observation noise,

$$\mathbf{Y}_t = \mathbf{Z}_t^{(1)} + \boldsymbol{\epsilon}_t,$$

with centered noise process $\boldsymbol{\epsilon}_t$, because it can otherwise be included into the dynamics of $\mathbf{Z}_t^{(1)}$.

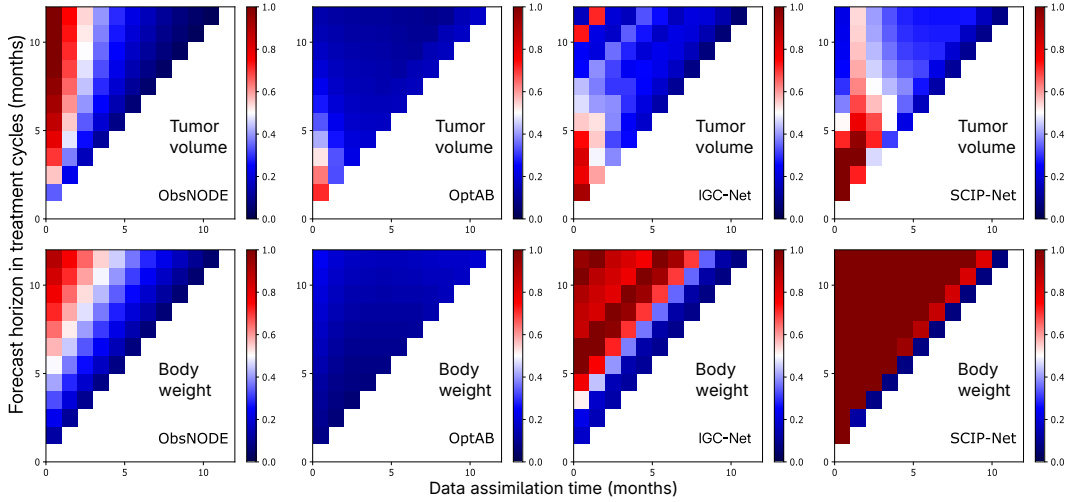


Figure 2: **Synthetic cancer dataset.** RMSE heatmaps (mean over five runs) for standardized (Z-score) tumor volume and body weight forecasts at confounding strength $\gamma = 4$. The horizontal axis shows the assimilation time and the vertical axis the forecast horizon. Columns correspond to ObsNODE, doseAI (Wendland, Kschischo, 2025), IGC-Net (Hess et al., 2026) and SCIP-Net (Hess, Feuerriegel, 2025). RMSE values larger than one were clipped at one.

4.3 Prediction and training of ObsNODEs

We approximate the filtering distribution $p(z_t | \mathbf{y}_t, \mathbf{o}_{[0,t]})$ with an RNN encoder, following Chen et al. (2018). Given the inferred state z_t , forecasts under a hypothetical treatment path $\mathbf{a}_{[t,t+s]}$ are obtained by integrating (5) forward in time and projecting to the observed space.

Training is self-supervised. For each unit, we choose a decision time t_c and provide observations up to t_c . The model then predicts future observations on $(t_c, t_f]$.

Observations are available only at irregular time points \mathcal{T}_{ij} . Let $\mathcal{T}_{ij}(t_c, t_f) = \mathcal{T}_{ij} \cap (t_c, t_f]$ denote the observation times of component j for unit i in that forecast window $(t_c, t_f]$. The predicted outcome vector for unit i and outcome component j at time t is to be compared against the corresponding observed value y_{tij}^{dat} in the training data. We minimize the masked squared error

$$\mathcal{L}_{(t_c, t_f]} = \sum_{i=1}^n \sum_{j=1}^{d_y} \frac{1}{n \sigma_j^2 |\mathcal{T}_{ij}(t_c, t_f)]|} \sum_{t \in \mathcal{T}_{ij}(t_c, t_f]} (y_{tij} - y_{tij}^{\text{dat}})^2,$$

where $|\mathcal{T}_{ij}(t_c, t_f)]|$ denotes the number of observations of component j for unit i in the forecasting interval $(t_c, t_f]$. This normalization compensates for varying observation frequencies across units and outcome components. The scaling factor σ_j^2 is the empirical variance of the j -th outcome component across all units and observed time points in the training data.

During training, a decision time $t_c \in [0, t_f)$ is selected for all units in a batch of size n and the corresponding losses $\mathcal{L}_{(t_c, t_f]}$ are averaged over different batches. We found that both a fixed set of possible values for t_c evenly distributed over $[0, t_f)$ or a uniform random choice led to very similar results. Choosing different decision times t_c in each batch exposes the model to varying assimilation times and forecast horizons.

5 Experiments

We evaluate ObsNODE on synthetic and semi-synthetic datasets where the ground-truth causal effect of a prescribed treatment path on the outcome trajectories is known and, in addition, on a real world data set. We compare against the IGC-Net (Hess et al., 2026), SCIP-Net (Hess, Feuerriegel, 2025) and two Treatment Effect Neural Controlled Differential Equation models (Seedat et al., 2022): optAB for

TUMOR VOLUME						
MODEL/ $s = t_f - t_c$	1	2	3	4	5	6
$\gamma = 4$						
OBSNODE	0.06±0.00	0.11±0.00	0.14±0.00	0.17±0.00	0.19±0.00	0.21±0.01
DOSEAI	0.16±0.02	0.15±0.02	0.12±0.01	0.12±0.01	0.11±0.00	0.10±0.01
IGC-NET	0.13±0.01	0.18±0.04	0.22±0.05	0.22±0.03	0.17±0.01	0.26±0.14
SCIP-NET	0.16±0.00	0.27±0.02	0.32±0.04	0.30±0.05	0.28±0.06	0.27±0.07
$\gamma = 6$						
OBSNODE	0.06±0.00	0.10±0.00	0.13±0.00	0.15±0.00	0.17±0.00	0.18±0.01
DOSEAI	0.12±0.02	0.11±0.01	0.10±0.01	0.10±0.01	0.10±0.00	0.10±0.01
IGC-NET	0.12±0.01	0.18±0.03	0.20±0.04	0.20±0.03	0.16±0.01	0.25±0.15
SCIP-NET	0.14±0.00	0.24±0.02	0.31±0.05	0.29±0.05	0.27±0.06	0.26±0.06
$\gamma = 8$						
OBSNODE	0.05±0.00	0.09±0.00	0.12±0.00	0.14±0.00	0.16±0.00	0.18±0.01
DOSEAI	0.12±0.01	0.11±0.00	0.11±0.00	0.11±0.01	0.12±0.01	0.13±0.02
IGC-NET	0.11±0.01	0.18±0.03	0.20±0.04	0.19±0.03	0.16±0.01	0.25±0.17
SCIP-NET	0.14±0.00	0.24±0.02	0.31±0.04	0.29±0.05	0.28±0.06	0.27±0.06

Table 1: **The RMSE for the tumor volume from synthetic data.** The RMSE between predicted and observed tumor volume (mean \pm std over five runs) for a fixed data assimilation time of $t_c = 5$ and different forecast horizons $s = t_f - t_c$ (in monthly treatment cycles) at different levels of confounding γ .

categorical treatments (Wendland et al., 2024) and doseAI for categorical and continuous treatments (Wendland, Kschischo, 2025).

Forecast root mean squared error (RMSE) was scaled with the standard deviation of each dynamic variable in the test set and is reported as a function of assimilation time (the duration of the treatment/observation history t_c) and prediction horizon (Figs. 2– 4). The RMSE values of these heatmaps are given in <https://github.com/JenniferJaschob/ObsNODE.git>. For synthetic and semi-synthetic data we vary the confounding strength γ . Results are averaged over five independent runs with disjoint training, validation, and test sets. Data generation details are provided in the appendix.

5.1 Experiments with fully-synthetic data

Data: The synthetic dataset is generated from a dynamic model of tumor volume (Geng et al., 2017) and body weight (Wendland, Kschischo, 2025) under chemotherapy and radiotherapy. The treatment vector \mathbf{a}_t represents chemo- and radiotherapy doses administered in monthly cycles, and the outcome \mathbf{y}_t consists of tumor volume and body weight.

To simulate time-dependent confounding, treatment probabilities depend on the mean tumor volume over the previous 15 days (Melnychuk et al., 2022). Patient heterogeneity is introduced by sampling tumor growth and treatment response parameters from predefined distributions (Appendix A.3.1).

Results: Figure 2 compares tumor volume and body weight forecast RMSE for $\gamma = 4$. Since the IGC-Net cannot handle continuous doses, the treatments were discretized into binary variables (Appendix A.3.1). All models require at least one treatment cycle of data assimilation for accurate tumor volume prediction.

For long forecast horizons doseAI achieves the lowest error, followed by ObsNODE and the IGC-Net. For short horizons ($\tau \leq 2$ cycles) ObsNODE typically yields the most accurate predictions.

Detailed RMSE values for the tumor volume at different confounding strengths γ and prediction horizons τ are reported in Table 1. ObsNODE consistently shows the smallest variance across different runs.

5.2 Experiments with semi-synthetic data

Data: The second experiment employs a semi-synthetic dataset derived from real-world medical data. The MIMIC-IV dataset (Johnson et al., 2023) serves as the foundation, with a focus on the patient cohort diagnosed with sepsis. Based on this patient cohort, synthetic data are generated to represent

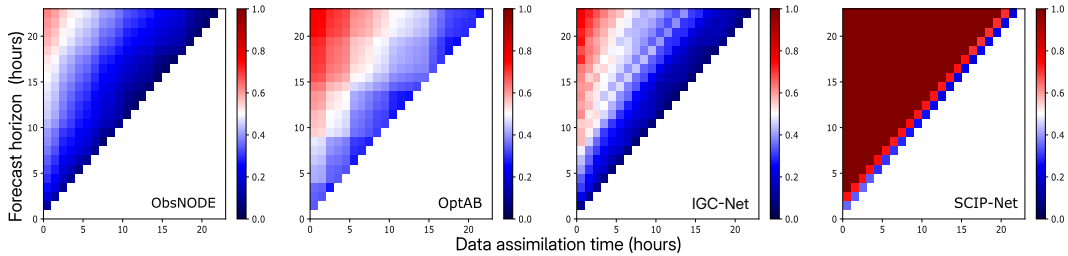


Figure 3: **Semi-synthetic MIMIC-IV sepsis dataset.** RMSE for ObsNODE, OptAB, IGC-Net and SCIP-Net as a function of data assimilation time (observation time) and forecast horizon over a 24-hour horizon. Results are averaged over five runs and RMSE values larger than one were clipped at one.

MODEL/ $s = t_f - t_c$	1	2	3	4	5	6
SEMI-SYNTHETIC OUTCOME						
OBSNODE	0.13±0.00	0.21±0.00	0.25±0.00	0.27±0.00	0.30±0.00	0.33±0.00
OPTAB	0.34±0.04	0.35±0.04	0.41±0.02	0.42±0.02	0.44±0.02	0.45±0.02
IGC-NET	0.10±0.03	0.21±0.01	0.25±0.01	0.29±0.02	0.34±0.02	0.38±0.01
SCIP-NET	0.34±0.10	0.73±0.10	1.32±0.16	1.32±0.16	1.33±0.16	1.32±0.16

Table 2: **Semi-synthetic MIMIC-IV sepsis dataset.** RMSE (mean \pm std over 5 runs) over a $s = t_f - t_c$ hour horizon when observing for a fixed data assimilation time of $t_c = 1$ hour.

patient trajectories and outcomes under both endogenous and exogenous dependencies, while explicitly incorporating treatment effects. The synthetic data generation methodology was originally defined using the MIMIC-III dataset (Schulam, Saria, 2018; Johnson et al., 2016; Melnychuk et al., 2022). Further details on the synthetic data generation process are provided in Appendix A.3.2.

Results: Figure 3 shows results on the semi-synthetic MIMIC-IV sepsis dataset. ObsNODE achieves consistently a low RMSE across the 24-hour prediction horizon and performs better than OptAB, IGC-Net and SCIP-Net for longer horizons. RMSE statistics averaged over five runs (Table 2) show very small variance for ObsNODE, indicating stable predictions compared to the baselines.

5.3 Experiments with real-world data

Data: Selecting antibiotic therapy for sepsis patients is challenging (Wendland et al., 2024). We use the Sequential Organ Failure Assessment (SOFA) score, a summary measure of organ dysfunction, as the primary outcome and predict the effects of the antibiotics vancomycin, ceftriaxone, and piperacillin-tazobactam on the SOFA trajectory. In addition, we predict treatment effects on the side-effect markers creatinine, total bilirubin, and alanine aminotransferase (ALT). Further dynamic variables included in the observation vector are listed in Table 7 in Appendix A.3.3 .

Results: Figure 4 compares the RMSE of ObsNODE forecasts with the OptAB, IGC-Net and SCIP-Net models. Apart from SCIP-Net, all other models predict the SOFA score reasonably well. IGC-Net performs well for very short term forecasts of the laboratory variables creatinine, total bilirubin, and ALT, but is outperformed by ObsNODE for longer forecast horizons.

Table 3 shows the five-run robustness analysis. Performance is measured by RMSE over a 6-hour prediction horizon, reporting mean and standard deviation across runs. ObsNODE predictions exhibit low variation across datasets sampled from the same distribution.

6 Related Work

Classical statistical approaches for longitudinal causal inference focus on estimating population-level average potential outcomes and do not condition on individual treatment and outcome histories (Robins, 1986; Bang, Robins, 2005; Lok, 2008; Van Der Laan, Gruber, 2012; Rytgaard et al.,

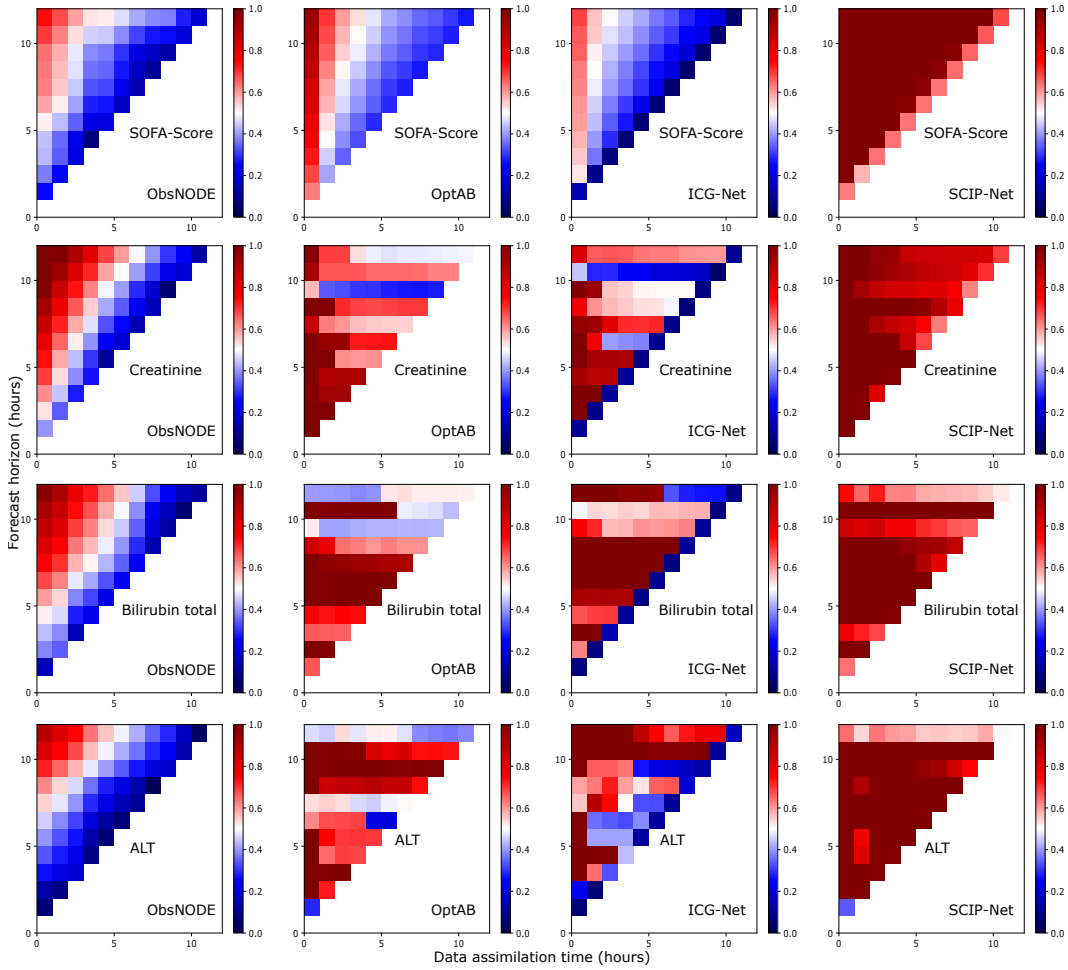


Figure 4: **Antibiotic sepsis treatment.** Forecast RMSE for SOFA score, creatinine, total bilirubin, and alanine aminotransferase (ALT) as a function of data assimilation time (x-axis) and forecast horizon (y-axis).

2022). Consequently, they cannot be used for individualized outcome forecasting. These approaches are typically grounded in structural causal models and identification results such as the longitudinal g-formula. Extensions to continuous time include structural dynamic causal models (Bongers et al., 2022), which adopt a different formulation of interventions than considered here. Recent work has developed discrete-time sequence models for estimating conditional average potential outcomes (CAPO) (i.e. the expectation value of (4)), including recurrent and attention-based architectures (Bica et al., 2020; Li et al., 2020; Melnychuk et al., 2022; Hess et al., 2026). A limitation of these approaches is their reliance on fixed time discretizations, whereas clinical measurements are typically observed at irregular time points.

Continuous-time approaches based on neural differential equations address this limitation. Treatment Effect Controlled Differential Equations (TE-CDEs) (Seedat et al., 2022) combine controlled differential equations (Kidger et al., 2020) with representation balancing to mitigate time-dependent confounding. The original formulation considered binary treatments and was later extended to continuous treatments (Wendland, Kschischo, 2025). However, balancing-based approaches may not fully address time-dependent confounding in sequential settings (Melnychuk et al., 2022).

The SCIP-Net (Hess, Feuerriegel, 2025) is a recent continuous time method for estimating the CAPO based on a stabilized inverse propensity score weighting, which is, however, restricted to discrete treatment levels.

MODEL/ $s = t_f - t_c$	1	2	3	4	5	6
SOFA-SCORE						
OBSNODE	0.24±0.00	0.32±0.01	0.37±0.01	0.42±0.02	0.47±0.03	0.50±0.04
OPTAB	0.41±0.01	0.46±0.01	0.50±0.02	0.53±0.02	0.57±0.02	0.59±0.02
IGC-NET	0.09±0.00	0.37±0.00	0.40±0.00	0.43±0.00	0.45±0.00	0.48±0.01
SCIP-NET	0.57±0.06	1.03±0.44	1.25±0.43	1.23±0.39	1.21±0.35	1.19±0.33
CREATININE						
OBSNODE	0.34±0.00	0.44±0.00	0.53±0.00	0.53±0.02	0.58±0.04	0.65±0.07
OPTAB	1.14±0.02	0.93±0.02	0.89±0.03	1.23±0.03	0.96±0.01	0.62±0.02
IGC-NET	0.09±0.02	1.13±0.01	0.89±0.00	0.92±0.01	0.78±0.15	0.95±0.01
SCIP-NET	1.01±0.04	1.06±0.26	1.36±0.28	1.39±0.30	1.17±0.39	0.99±0.42
BILIRUBIN-TOTAL						
OBSNODE	0.34±0.00	0.38±0.00	0.46±0.02	0.54±0.04	0.62±0.07	0.70±0.11
OPTAB	1.36±0.05	0.66±0.01	0.73±0.07	1.05±0.04	1.56±0.14	0.97±0.05
IGC-NET	0.07±0.01	1.40±0.02	0.69±0.01	0.91±0.00	1.07±0.01	1.59±0.03
SCIP-NET	1.23±0.17	0.72±0.12	1.13±0.11	1.24±0.12	1.84±0.14	1.17±0.14
ALT						
OBSNODE	0.09±0.00	0.22±0.01	0.27±0.03	0.33±0.06	0.39±0.10	0.47±0.13
OPTAB	0.72±0.20	1.25±0.09	0.65±0.16	0.76±0.25	0.67±0.21	0.54±0.11
IGC-NET	0.06±0.02	0.64±0.17	1.34±0.21	0.41±0.02	0.36±0.03	0.90±0.23
SCIP-NET	1.75±0.20	1.51±0.30	0.81±0.28	0.77±0.37	2.24±0.45	1.45 ± 0.26

Table 3: **Robustness analysis on the MIMIC-IV sepsis dataset.** RMSE for different prediction horizons (in hours) and a fixed data assimilation time of $t_c = 1$ hour. Mean and standard deviation are reported across five runs.

Our ObsNODE framework is most closely related to CF-ODE (Brouwer et al., 2022), which parameterizes a continuous-time state-space model of the form (3) using a Neural ODE. CF-ODE assumes that observations at treatment time uniquely determine the latent state, corresponding to the observability condition (Definition 3.1). However, this assumption is not structurally enforced and is difficult to verify in practice. In contrast, ObsNODE employs the observable normal form (5), which guarantees observability by construction and makes explicit the link between control-theoretic observability and the identifiability condition required for the causal adjustment formula (4). Moreover, CF-ODE conditions only on prior observations and does not explicitly incorporate the treatment history.

Together, these limitations motivate a continuous-time state-space formulation that enforces observability and enables causal outcome prediction through an explicit adjustment formula, which we develop in the ObsNODE framework.

7 Conclusion and Limitations

We introduced Observable Neural ODEs (ObsNODE), a continuous-time framework for causal forecasting under sequential treatments. By combining Neural ODE dynamics with an observable latent-state representation, ObsNODE enables identification of treatment effects under time-varying treatments and hidden confounding while modeling latent disease dynamics. We further derived an adjustment formula for continuous-time causal forecasting. Experiments on synthetic, semi-synthetic, and real-world clinical data demonstrate strong performance compared to recent sequence models. As with all causal models, the approach relies on assumptions about the data-generating process. In particular, hidden confounders may affect treatments and observed variables, but are assumed not to directly alter the latent disease dynamics. We consider these assumptions comparatively mild within the state-space setting, although their validity in real-world multimodal data requires further study. The adjustment formula also provides a basis for uncertainty quantification of causal forecasts.

Acknowledgments and Disclosure of Funding

References

Adamy Jürgen. Nonlinear Systems and Controls. Berlin, Heidelberg: Springer Berlin Heidelberg,

2024. 2. 2nd ed. 2024.

- Bang Heejung, Robins James M.* Doubly Robust Estimation in Missing Data and Causal Inference Models // *Biometrics*. XII 2005. 61, 4. 962–973.
- Bernard Pauline.* Observer Design for Nonlinear Systems. 479. Cham: Springer International Publishing, 2019. (Lecture Notes in Control and Information Sciences).
- Bica Ioana, Alaa Ahmed M., Jordon James, Schaar Mihaela van der.* Estimating Counterfactual Treatment Outcomes over Time Through Adversarially Balanced Representations. II 2020.
- Bongers Stephan, Blom Tineke, Mooij Joris M.* Causal Modeling of Dynamical Systems // arXiv.org preprint. III 2022. arXiv:1803.08784v4 [cs.AI].
- Brouwer Edward De, Hernández Javier González, Hyland Stephanie.* Predicting the impact of treatments over time with uncertainty aware neural differential equations. II 2022.
- Chen Ricky T. Q., Rubanova Yulia, Bettencourt Jesse, Duvenaud David K.* Neural Ordinary Differential Equations // *Advances in Neural Information Processing Systems*. 31. 2018.
- Geng Changran, Paganetti Harald, Grassberger Clemens.* Prediction of Treatment Response for Combined Chemo- and Radiation Therapy for Non-Small Cell Lung Cancer Patients Using a Bio-Mathematical Model // *Scientific Reports*. X 2017. 7, 1. 13542.
- Goldberger Ary L., Amaral Luis A. N., Glass Leon, Hausdorff Jeffrey M., Ivanov Plamen Ch, Mark Roger G., Mietus Joseph E., Moody George B., Peng Chung-Kang, Stanley H. Eugene.* PhysioBank, PhysioToolkit, and PhysioNet // *Circulation*. VI 2000.
- Hensman James, Durrande Nicolas, Solin Arno.* Variational Fourier Features for Gaussian Processes // *Journal of Machine Learning Research*. 2018. 18, 151. 1–52.
- Hernán Miguel, Robins James M.* Causal inference: what if. Boca Raton: Taylor and Francis, 2023. First edition.
- Hess Konstantin, Feuerriegel Stefan.* Stabilized Neural Prediction of Potential Outcomes in Continuous Time. 2025.
- Hess Konstantin, Frauen Dennis, Melnychuk Valentyn, Feuerriegel Stefan.* IGC-Net for conditional average potential outcome estimation over time // *The Fourteenth International Conference on Learning Representations*. 2026.
- Hofford Mackenzie R, Yu Sean C, Johnson Alistair E W, Lai Albert M, Payne Philip R O, Michelson Andrew P.* OpenSep: a generalizable open source pipeline for SOFA score calculation and Sepsis-3 classification // *JAMIA Open*. XII 2022. 5, 4. ooac105.
- Jazwinski Andrew H.* Stochastic processes and filtering theory. Mineola, N.Y: Dover Publications, 2007. Dover ed. (Dover books on engineering).
- Johnson Alistair E. W., Bulgarelli Lucas, Shen Lu, Gayles Alvin, Shammout Ayad, Horng Steven, Pollard Tom J., Hao Sicheng, Moody Benjamin, Gow Brian, Lehman Li-wei H., Celi Leo A., Mark Roger G.* MIMIC-IV, a freely accessible electronic health record dataset // *Scientific Data*. I 2023. 10, 1. 1.
- Johnson Alistair E. W., Pollard Tom J., Shen Lu, Lehman Li-Wei H., Feng Mengling, Ghassemi Mohammad, Moody Benjamin, Szolovits Peter, Celi Leo Anthony, Mark Roger G.* MIMIC-III, a freely accessible critical care database // *Scientific Data*. V 2016. 3. 160035.
- Jong Johann de, Emon Mohammad Asif, Wu Ping, Karki Reagon, Sood Meemansa, Godard Patrice, Ahmad Ashar, Vrooman Henri, Hofmann-Apitius Martin, Fröhlich Holger.* Deep learning for clustering of multivariate clinical patient trajectories with missing values // *GigaScience*. XI 2019. 8, 11. giz134.
- Kidger Patrick, Morrill James, Foster James, Lyons Terry.* Neural Controlled Differential Equations for Irregular Time Series. XI 2020.

- Li Rui, Shahn Zach, Li Jun, Lu Mingyu, Chakraborty Prithwish, Sow Daby, Ghalwash Mohamed, Lehman Li-wei H.* G-Net: A Deep Learning Approach to G-computation for Counterfactual Outcome Prediction Under Dynamic Treatment Regimes. III 2020.
- Lok Judith J.* Statistical modeling of causal effects in continuous time // *Ann. Statist.* VI 2008. 36, 3.
- Melnychuk Valentyn, Frauen Dennis, Feuerriegel Stefan.* Causal Transformer for Estimating Counterfactual Outcomes. VI 2022.
- Murphy S. A.* Optimal Dynamic Treatment Regimes // *Journal of the Royal Statistical Society Series B: Statistical Methodology.* IV 2003. 65, 2. 331–355. _eprint: https://academic.oup.com/jrsssb/article-pdf/65/2/331/4968441/jrsssb_65_2_331.pdf.
- Pearl Judea.* Causality: models, reasoning, and inference. Cambridge, U.K. ; New York: Cambridge University Press, 2000.
- Peters Jonas, Janzing Dominik, Schölkopf Bernhard.* Elements of causal inference: foundations and learning algorithms. Cambridge, Mass: The MIT press, 2017. (Adaptive computation and machine learning).
- Robins James.* A new approach to causal inference in mortality studies with a sustained exposure period—application to control of the healthy worker survivor effect // *Mathematical Modelling.* I 1986. 7, 9. 1393–1512.
- Robins James M.* Optimal Structural Nested Models for Optimal Sequential Decisions // *Proceedings of the Second Seattle Symposium in Biostatistics: Analysis of Correlated Data.* New York, NY: Springer New York, 2004. 189–326.
- Rubanova Yulia, Chen Ricky T. Q., Duvenaud David.* Latent ODEs for Irregularly-Sampled Time Series. 2019.
- Rubin Donald B.* Randomization Analysis of Experimental Data: The Fisher Randomization Test Comment // *Journal of the American Statistical Association.* IX 1980. 75, 371. 591.
- Rytgaard Helene C., Gerds Thomas A., Van Der Laan Mark J.* Continuous-time targeted minimum loss-based estimation of intervention-specific mean outcomes // *Ann. Statist.* X 2022. 50, 5.
- Schulam Peter, Saria Suchi.* Reliable Decision Support using Counterfactual Models. II 2018.
- Seedat Nabeel, Imrie Fergus, Bellot Alexis, Qian Zhaozhi, Schaar Mihaela van der.* Continuous-Time Modeling of Counterfactual Outcomes Using Neural Controlled Differential Equations. 2022.
- Van Der Laan Mark J., Gruber Susan.* Targeted Minimum Loss Based Estimation of Causal Effects of Multiple Time Point Interventions // *The International Journal of Biostatistics.* V 2012. 8, 1.
- Vincent J. L., Moreno R., Takala J., Willatts S., De Mendonça A., Bruining H., Reinhart C. K., Suter P. M., Thijs L. G.* The SOFA (Sepsis-related Organ Failure Assessment) score to describe organ dysfunction/failure. On behalf of the Working Group on Sepsis-Related Problems of the European Society of Intensive Care Medicine // *Intensive Care Medicine.* VII 1996. 22, 7. 707–710.
- Wendland Philipp, Birkenbihl Colin, Gomez-Freixa Marc, Sood Meemansa, Kschischo Maik, Fröhlich Holger.* Generation of realistic synthetic data using Multimodal Neural Ordinary Differential Equations // *npj Digital Medicine.* VIII 2022. 5, 1. 122.
- Wendland Philipp, Kschischo Maik.* Dynamic Dose Optimization Under Side Effect Constraints Using Counterfactual Outcome Prediction // *Artificial Intelligence in Medicine.* 15735. Cham: Springer Nature Switzerland, 2025. 428–433. Series Title: Lecture Notes in Computer Science.
- Wendland Philipp, Schenkel-Häger Christof, Wenningmann Ingobert, Kschischo Maik.* An optimal antibiotic selection framework for Sepsis patients using Artificial Intelligence // *NPJ digital medicine.* XI 2024. 7, 1. 343.
- Xu Ziqi, Cheng Debo, Li Jiuyong, Liu Jixue, Liu Lin, Yu Kui.* Causal Inference with Conditional Front-Door Adjustment and Identifiable Variational Autoencoder // *The Twelfth International Conference on Learning Representations.* 2024.

A Technical Appendix and Supplementary Material

A.1 Derivation of equation (4)

In the main text we derived only a discrete version of the adjustment formula (4) and here we provide the continuous time version. Assume we have observed a treatment and outcome history $\mathbf{o}_{[0,t)} = \{\mathbf{a}_{[0,t)}, \mathbf{y}_{[0,t)}\}$ before time t and also the outcome $\mathbf{Y}_t = \mathbf{y}_t$ at time t . We want to compute the probability density $P_{\mathbf{Y}_{t+s}(\mathbf{a}_{[t,t+s)})|\mathbf{Y}_t, \mathbf{o}_{[0,t)}(\mathbf{y}_{t+s}|\mathbf{y}_t, \mathbf{o}_{[0,t)})}$ for the potential outcome $\mathbf{Y}_{t+s}(\mathbf{a}_{[t,t+s)})$ under the hypothetical intervention path $\mathbf{a}_{[t,t+s)}$ applied in the time interval $[t, t+s)$.

Let us partition the data assimilation time interval $[0, t)$ into K subintervals $[t_k, t_{k+1})$ with $t_0 = 0, t_K = t$ and $[0, t) = \cup_{k=1}^K [t_k, t_{k+1})$. Similarly, partition the prediction interval $[t, t+s)$ into L subintervals with $[t_l, t_{l+1})$ with $t_{K+1} = t, t_{K+L} = t+s$ and $[t, t+s) = \cup_{l=K+1}^{K+L} [t_l, t_{l+1})$.

For each $t_k \in [0, t)$ and $t_l \in [t, t+s)$ we identify the variables in the CFD (2) with variables in our model as

$$A \leftarrow \mathbf{A}_{t_k}, \quad Y \leftarrow \mathbf{Y}_{t_l}, \quad M \leftarrow \mathbf{Z}_{t_l}, \quad W \leftarrow \{\mathbf{Z}_t, \mathbf{Y}_t, \mathbf{A}_{t_k}, \mathbf{Y}_{t_k}\} = \{\mathbf{Z}_t, \mathbf{Y}_t, \mathbf{O}_{t_k}\},$$

with $\mathbf{O}_{t_k} = \{\mathbf{A}_{t_k}, \mathbf{Y}_{t_k}\}$. We can check graphically (replace t_k by 0 and t_l by $t+s$ in Fig. 1) that $M = \mathbf{Z}_{t_l}$ fulfills the CFD 3.2 with respect to $(A, Y) = (\mathbf{A}_{t_k}, \mathbf{Y}_{t_l})$ with the conditioning variables $W = \{\mathbf{Z}_t, \mathbf{Y}_t, \mathbf{O}_{t_k}\}$.

In order to apply the CFD to sets of variables we define

$$\mathbf{A}_{0:K} := \{\mathbf{A}_{t_k} | t_k \in [0, t)\}, \quad \mathbf{Y}_{0:K} := \{\mathbf{Y}_{t_k} | t_k \in [0, t)\}, \quad \mathbf{A}_{K+1:L} := \{\mathbf{A}_{t_l} | t_l \in [t, t+s)\}.$$

Selecting the following sets in Theorem 3.2

$$A \leftarrow \mathbf{A}_{K+1:L}, \quad Y \leftarrow \mathbf{Y}_{t+s}, \quad M \leftarrow \mathbf{Z}_{t+s}, \quad W \leftarrow \{\mathbf{Z}_t, \mathbf{Y}_t, \mathbf{A}_{0:K}, \mathbf{Y}_{0:K}\} = \{\mathbf{Z}_t, \mathbf{Y}_t, \mathbf{O}_{0:K}\},$$

we see that $M = \mathbf{Z}_{t+s}$ fulfills the CFD relative to $(A, Y) = (\mathbf{A}_{K+1:L}, \mathbf{Y}_{t+s})$ with the conditioning set $W = \{\mathbf{Z}_t, \mathbf{Y}_t, \mathbf{O}_{0:K}\}$. Applying the adjustment formula of the CFD (2) we have for the probability density of the potential outcome \mathbf{Y}_{t+s} under the treatment sequence $\mathbf{a}_{K+1:L}$

$$\begin{aligned} P_{\mathbf{Y}_{t+s}(\mathbf{A}_{K+1:L})}(\mathbf{y}_{t+s}) &= \int_{\mathbf{z}_{t+s}} \int_{\mathbf{a}'_{K+1:L}} \int_{\mathbf{z}_t, \mathbf{y}_t, \mathbf{o}_{0:K}} \{p(\mathbf{y}_{t+s} | \mathbf{a}'_{K+1:L}, \mathbf{z}_{t+s}, \mathbf{z}_t, \mathbf{y}_t, \mathbf{o}_{0:K}) \\ &\quad \times p(\mathbf{a}'_{K+1:L} | \mathbf{z}_t, \mathbf{y}_t, \mathbf{o}_{0:K}) p(\mathbf{z}_{t+s} | \mathbf{a}_{K+1:L}, \mathbf{z}_t, \mathbf{y}_t, \mathbf{o}_{0:K}) p(\mathbf{z}_t, \mathbf{y}_t, \mathbf{o}_{0:K})\}. \end{aligned}$$

Now we use the independence relations implied by the state space model (3)

$$\begin{aligned} P(\mathbf{y}_{t+s} | \mathbf{a}'_{K+1:L}, \mathbf{z}_{t+s}, \mathbf{z}_t, \mathbf{y}_t, \mathbf{o}_{0:K}) &= p(\mathbf{y}_{t+s} | \mathbf{z}_{t+s}) \\ p(\mathbf{z}_{t+s} | \mathbf{a}_{K+1:L}, \mathbf{z}_t, \mathbf{y}_t, \mathbf{o}_{0:K}) &= p(\mathbf{z}_{t+s} | \mathbf{a}_{K+1:L}, \mathbf{z}_t) \end{aligned}$$

and find for the probability density of the potential outcome

$$\begin{aligned} P_{\mathbf{Y}_{t+s}(\mathbf{A}_{K+1:L})}(\mathbf{y}_{t+s}) &= \int_{\mathbf{z}_{t+s}} \int_{\mathbf{a}'_{K+1:L}} \int_{\mathbf{z}_t, \mathbf{y}_t, \mathbf{o}_{0:K}} \{p(\mathbf{y}_{t+s} | \mathbf{z}_{t+s}) \\ &\quad \times p(\mathbf{a}'_{K+1:L} | \mathbf{z}_t, \mathbf{y}_t, \mathbf{o}_{0:K}) p(\mathbf{z}_{t+s} | \mathbf{a}_{K+1:L}, \mathbf{z}_t) p(\mathbf{z}_t, \mathbf{y}_t, \mathbf{o}_{0:K})\} \\ &= \int_{\mathbf{z}_{t+s}} \int_{\mathbf{z}_t, \mathbf{y}_t, \mathbf{o}_{0:K}} p(\mathbf{y}_{t+s} | \mathbf{z}_{t+s}) p(\mathbf{z}_{t+s} | \mathbf{a}_{K+1:L}, \mathbf{z}_t) p(\mathbf{z}_t | \mathbf{y}_t, \mathbf{o}_{0:K}) p(\mathbf{y}_t, \mathbf{o}_{0:K}). \end{aligned}$$

From this, we read

$$P_{\mathbf{Y}_{t+s}(\mathbf{a}_{K+1:L})|\mathbf{Y}_t, \mathbf{o}_{0:K}}(\mathbf{y}_{t+s} | \mathbf{y}_t, \mathbf{o}_{0:K}) \tag{6}$$

$$= \int_{\mathbf{z}_{t+s}} \int_{\mathbf{z}_t} p(\mathbf{y}_{t+s} | \mathbf{z}_{t+s}) p(\mathbf{z}_{t+s} | \mathbf{a}_{K+1:L}, \mathbf{z}_t) p(\mathbf{z}_t | \mathbf{y}_t, \mathbf{o}_{0:K}). \tag{7}$$

This formula is valid for any partitions of the data assimilation interval $[0, t)$ and the forecast interval $[t, t+s)$. Making the partitions finer and finer by sending $K \rightarrow \infty$ and $L \rightarrow \infty$ allows us to replace $\mathbf{o}_{0:K}$ and by $\mathbf{o}_{[0,t)}$ and $\mathbf{a}_{K+1:L}$ by $\mathbf{a}_{[t,t+s)}$ and we obtain (4). The model forecast is deterministic in (3) and we have $p(\mathbf{z}_{t+s} | \mathbf{a}_{[t,t+s)}, \mathbf{z}_t) = \delta\left(\mathbf{z}_{t+s} - \mathbf{z}_t - \int_t^{t+s} \mathbf{f}(\mathbf{z}_\tau, \mathbf{a}_\tau) d\tau\right)$.

Applying the continuum limit in (6) only to the hypothetical treatment trajectory ($L \rightarrow \infty$) we have

$$\begin{aligned} & P_{\mathbf{Y}_{t+s}(\mathbf{a}_{[t,t+s]})|\mathbf{Y}_t, \mathbf{o}_{0:K}}(\mathbf{y}_{t+s}|\mathbf{y}_t, \mathbf{o}_{0:K}) \\ &= \int_{\mathbf{z}_{t+s}} \int_{\mathbf{z}_t} p(\mathbf{y}_{t+s}|\mathbf{z}_{t+s})p(\mathbf{z}_{t+s}|\mathbf{a}_{[t,t+s]}, \mathbf{z}_t)p(\mathbf{z}_t|\mathbf{y}_t, \mathbf{o}_{0:K}). \end{aligned}$$

If the discretization time points $t_k \in [0, t)$ for the data assimilation interval $[0, t)$ coincide with the time points for the observed data, we have an adjustment formula for discrete time observations and continuous time treatment trajectories. Here, $p(\mathbf{z}_t|\mathbf{y}_t, \mathbf{o}_{0:K})$ is the filtering distribution for the continuous time ODE model 3 with discrete time observations (Jazwinski, 2007).

A.2 Details on training the ObsNODE model

The datasets were split into training, validation, and test sets and feature-wise Z-score normalization was applied using statistics computed on the training set only. The normalized dataset is subsequently used for model training.

Each multivariate time series was segmented at a decision time point t_c into two disjoint subsequences. The prefix segment consists of all observations prior to t_c and is used to condition the recognition model. The model infers an initial state \mathbf{z}_0 for each individual trajectory using an LSTM-based recognition network Rubanova et al. (2019).

To handle missing observations, the recognition LSTM is augmented with an explicit imputation mechanism. The indicator function

$$\mathcal{I}_{tij} = \begin{cases} 1 & : y_{tij} \text{ is observed} \\ 0 & : y_{tij} \text{ is missing.} \end{cases}$$

indicates whether the data for the j -th component of the i -th unit at time t is observed or not, The imputation layer is defined as the transformation

$$y_{tij} = y_{tij} \cdot \mathcal{I}_{tij} + b_j \cdot (1 - \mathcal{I}_{tij}),$$

where b_j are learnable parameters Jong de et al. (2019); Wendland et al. (2022). This formulation replaces missing entries with trainable values that are optimized jointly with the LSTM parameters in an end-to-end fashion.

The latent initial states \mathbf{z}_0 inferred by the LSTM, together with the control function \mathbf{a}_t are subsequently passed as inputs to the Neural Differential Equation (NODE) model. The observations after the decision time point t_c are used for loss computation and subsequent optimization. Model parameters are optimized using the Adam optimizer.

The ObsNODE model supports both direct long-horizon forecasting and a recursive scheme, similar in spirit to ODE-RNN Rubanova et al. (2019). In the long-horizon setting, the state estimated by the LSTM recognition model is used to generate a forecast over the entire prediction window. In the recursive setting, forecasts are produced iteratively: at each step, the ODE model generates a short-term prediction, which is appended to the observation and treatment history sequence observed up to t_c . Conditioned on this augmented sequence, the LSTM updates the latent state, which then serves as the initial condition for the next ODE rollout. This process repeats until the full horizon is covered, without using any ground-truth observations beyond t_c . We find empirically that augmenting the sequence with intermediate predictions can improve stability for longer forecasting horizons in some settings.

A.2.1 Code availability

ObsNODE is implemented in PyTorch. Code is available at <https://github.com/JenniferJaschob/ObsNODE.git>. The repository includes scripts for data preprocessing, simulation, model training, and evaluation, together with configuration files specifying all hyperparameters used in the experiments.

A.3 Details for Computational Experiments

A.3.1 Details for Synthetic Data Simulation

The synthetic data set is simulated from a dynamic model for tumor volume $V(t)$ (in cm^3) (Geng et al., 2017; Bica et al., 2020) and net body weight $W^{net}(t)$ (in kg) in response to a dynamic dosing trajectory for chemotherapy $C(t)$ and radiotherapy $d(t)$ combination treatment (Wendland, Kschischo, 2025):

$$\frac{dV(t)}{dt} = \left(\rho \log \left(\frac{K}{V(t)} \right) - \beta_c C(t) - \left(\alpha_r d(t) + \beta_r d(t)^2 \right) + \epsilon(t) \right) V(t) \quad (8a)$$

$$\frac{dW^{net}(t)}{dt} = k_g W^{net}(t) \left(1 - \frac{W^{net}(t)}{G} \right) - \beta_{wc} C(t) - \alpha_{wr} d(t) - \lambda V(t). \quad (8b)$$

The tumor volume is assumed to follow a Gompertz growth function, which is inhibited by the chemotherapy and radiotherapy dosing. The Gaussian zero mean white noise process $\epsilon(t)$ renders the tumour volume a stochastic variable.

Net body weight $W^{net}(t)$ is modeled as a logistic growth process, modified by tumor volume and therapy-induced weight loss (Wendland, Kschischo, 2025). Net body weight $W^{net}(t) = W(t) - \rho_d V(t)$ is defined as body weight $W(t)$ minus the tumor weight, with ρ_d denoting the tumor density. The parameter G corresponds to the saturation level, which in this case is set to the initial weight. The parameters β_{wc} , α_{wr} , and λ determine the weight loss contributions of chemotherapy, radiotherapy, and disease impact, respectively.

Treatment doses are modeled as time dependent random variables

$$C(t) = C_{max} \sigma \left(\frac{\gamma_c * \alpha_c^{dose}}{D_{max}} (\bar{D}(t) - \delta_c) \right) \quad (9a)$$

$$d(t) = d_{max} \sigma \left(\frac{\gamma_r * \alpha_r^{dose}}{D_{max}} (\bar{D}(t) - \delta_r) \right), \quad (9b)$$

where σ is the softmax function and $C_{max} = 14 \text{ mg/m}^3$ and $d_{max} = 3 \text{ Gy}$ are the maximum doses for for chemo- and radiotherapy, respectively. The prescribed treatment doses depend on the outcome via the mean tumor diameter $\bar{D}(t)$ over the last 15 days (Melnychuk et al., 2022). The parameter $D_{max} = 13 \text{ cm}$ is the maximum tumor diameter and we set $\delta_c = \delta_r = \frac{D_{max}}{2}$. The degree of time dependent confounding is given by the parameters γ_c and γ_r , with range $\gamma = \gamma_c = \gamma_r \in [1, 8]$. The values of α_c^{dose} and α_r^{dose} are sampled uniformly in the range from 1cm to 4cm to simulate variability in individual dosing decisions. The IGC-Net model can only process binary treatments indicators \mathbf{a}_t and we interpret $C(t)/C_{max}$ and $d(t)/d_{max}$ for IGC-Net as probabilities for the Bernoulli-variables of treatment for chemo- and radiotherapy, respectively.

We simulate 3,000 patients and use 1,000 patients each for training, validation, and testing. Chemotherapy dose $C(t)$ and radiotherapy dose $d(t)$ was adjusted in monthly treatment cycles by sampling from (9). To model patient variability, we sampled patient specific parameters from Gaussian distributions, see Table 4.

A.3.2 Details for Semi-Synthetic Data Simulation

To generate semi-synthetic data (Schulam, Saria, 2018) we have modified the approach from (Melnychuk et al., 2022). We use the sepsis patient cohort (3557 patients) from the MIMIC-IV dataset (Johnson et al., 2023) (see also A.3.3) and select three vital signs as time dependent hidden confounders ϵ_t . Then, we simulate untreated outcomes $j \in \{1, \dots, d_y\}$ as

$$\tilde{Y}_t^{j,(i)} = \alpha_s^j B\text{-spline}(t) + \alpha_g^j g^{j,(i)}(t) + \alpha_\phi^j \phi_Y^j(\epsilon_t^{(i)}) + \eta_t^{j,(i)} \quad (10)$$

with noise $\eta_t^{j,(i)} \sim \mathcal{N}(0, 0.005^2)$ and weight coefficients α_s^j , α_g^j and α_ϕ^j . The term $B\text{-spline}(t)$ represents a mixture of three cubic B-splines. The function $g^{j,(i)}$ is independently sampled for each patient i from a Gaussian process with a Matérn kernel, and ϕ_Y^j is sampled via random Fourier features (RFF) (Hensman et al., 2018).

MODEL	VARIABLE	PARAMETER	DISTRIBUTION	DISTRIBUTION VALUE (μ, σ)
TUMOR	GROWTH PARAMETER	ρ	NORMAL	$7 \times 10^{-5}, 0.00723$
TUMOR	CARRYING CAPACITY	K	CONSTANT	30
TUMOR	RADIO CELL KILL (α)	α_r	NORMAL	0.0398, 0.168
TUMOR	RADIO CELL KILL (β)	β_r	-	SET $\alpha/\beta = 10$
TUMOR	CHEMO CELL KILL	β_c	NORMAL	0.028, 0.0007
TUMOR	NOISE	ϵ_{vt}	NORMAL	0, 0.01
WEIGHT	GROWTH PARAMETER	ρ_w	NORMAL	$14 \times 10^{-5}, 10^{-5}$
WEIGHT	CARRYING CAPACITY	K_w	CONSTANT	INITIAL WEIGHT
WEIGHT	RADIO INFLUENCE	α_{wr}	NORMAL	0.004125, 10^{-4}
WEIGHT	CHEMO INFLUENCE	β_{wc}	NORMAL	0.001775, 2×10^{-4}
WEIGHT	CANCER INFLUENCE	λ	NORMAL	$31 \times 10^{-5}, 15 \times 10^{-6}$
WEIGHT	NOISE	ϵ_{wt}	NORMAL	0, 0.0015

Table 4: Parameter of the cancer growth simulation model (Wendland, Kschischo, 2025).

Synthetic binary treatments $\mathbf{A}_t = (A_t^1, \dots, A_t^{d_a}) \in \{0, 1\}^{d_a}$ with confounding are simulated via

$$A_t^l \sim \text{Bernoulli}(P_{A_t^l}), \quad P_{A_t^l} = \sigma\left(\gamma_A^l \bar{Y}_{t-1}^{A,l} + \gamma_\epsilon^l \Phi_\epsilon^l(\epsilon_t) + b_l\right),$$

where σ is the sigmoid function. The treatment probability $P_{A_t^l}$ for the l -th treatment component A_t^l depends on the outcome history, represented by an average over a subset of the previous treated outcomes $\bar{Y}_{t-1}^{A,l}$ Melnychuk et al. (2022). Hidden confounding of the treatment is represented via the function Φ_ϵ^l sampled from a RFF approximation of a Gaussian process. The parameters γ_A^l and γ_ϵ^l control the confounding strength and b_l is a bias parameter.

The time dependent treatment effect

$$E_t^j = \sum_{k=t-w^l}^t \frac{\min_{l=1, \dots, d_a} \mathbf{1}_{[A_k^l=1]} P_{A_k^l} \beta_{lj}}{(w^l - k)^2}. \quad (11)$$

is bounded by the maximum effect size $\beta_{lj} \in \{0, \beta\}$ of treatment component l on outcome j . It is either zero for outcomes j not affected by treatment l or equals the constant β . Finally, the treated outcomes are obtained from the untreated outcomes (10) by adding the treatment effects

$$Y_t^{j,(i)} = \tilde{Y}_t^{j,(i)} + E_t^j. \quad (12)$$

Parameters for the semi-synthetic sepsis data are given in Table 5.

Variable	Parameter	Value
Outcome	α	2
Outcome	α_g	0.5
Outcome	α_e	1
Outcome	ν	20
Outcome	Exogeneous Variables	Creatinine, Bilirubin, ALT
Treatment 1; 2	γ_z	0.3; 0.3
Treatment 1; 2	γ_0	0.3; 0.1
Treatment 1; 2	bias	-2; -2
Treatment 1; 2	ν	20; 20
Treatment 1; 2	Confounding Variables	Creatinine; Bilirubin, ALT

Table 5: Parameters of the data-simulation model for semi-synthetic data (Wendland, Kschischo, 2025).

A.3.3 Details on Experiments with Real-World Data

We use the MIMIC-IV electronic health record dataset collected at Beth Israel Deaconess Medical Center, which contains data from approximately 450,000 hospital admissions (Johnson et al., 2023).

ORGAN	PARAMETER	UNIT	1	2	3	4
RESPIRATION	PaO_2/FiO_2	<i>mmHg</i>	<400	<300	<200	<100
COAGULATION	PLATELETS	μl	<150.000	<100.00	<50.000	<20.000
LIVER	BILIRUBIN	MG/DL	1.2-1.9	2.0-5.9	6.0-11.9	>12.0
CARDIO-VASCULAR	MAP OR VASOPRESSORS	MMHG OR $\mu g/kg/min$	MAP < 70	DOPAM. \leq 5 OR DOBUTAM.	DOPAM. > 5 OR EPINEPH. \leq 0.1 OR NOREPIN. \leq 0.1	DOPAM. > 15 OR EPINEPH. > 0.1 OR NOREPIN. > 0.1
CENTRAL NERVOUS SYSTEM	GCS		13-14	10-12	6-9	<6
RENAL	CREATININE	MG/DL OR ML/D	1.2-1.9	2.0-3.4	3.5-4.9 OR URIN < 500	>5.9

Table 6: **Overview of the SOFA score subscores** (Wendland et al., 2024) Each column corresponds to a subscore (0–4) reflecting the severity of dysfunction in the central nervous, cardiovascular, respiratory, coagulation, hepatic, and renal systems. Subscores of 0 indicate normal organ function as defined by the respective criteria.

The dataset includes demographic information, laboratory values, vital signs, medications, and diagnoses.

For our analysis we focus on sepsis patients identified using the OpenSep pipeline according to the Sepsis-3 criteria (Hofford et al., 2022). Sepsis cases were defined by an increase in the Sequential Organ Failure Assessment (SOFA) score of at least two points within 48 hours before or 24 hours after a suspected infection.

The SOFA score is used as the clinical outcome variable. It summarizes dysfunction in six organ systems (respiratory, cardiovascular, central nervous system, coagulation, liver, and kidney), each scored from 0 to 4 according to the severity of dysfunction (Vincent et al., 1996). An overview of the subscores is given in Table 6.

We consider patients treated with the antibiotics vancomycin, ceftriaxone, and piperacillin-tazobactam. To assess potential treatment side effects we additionally predict laboratory indicators of organ toxicity, including creatinine (kidney injury) as well as total bilirubin and alanine aminotransferase (ALT) (liver injury).

Data preprocessing follows the OptAB pipeline (Wendland et al., 2024). The cohort is restricted to ICU patients, and antibiotic treatments are encoded as a vector of three binary variables indicating administration of vancomycin, ceftriaxone, and piperacillin-tazobactam.

Time-dependent covariates were selected from all available dynamic variables by excluding variables recorded in fewer than 50% of patients and retaining those with an absolute Spearman correlation of at least 0.3 with the SOFA score during the first 12 hours. The resulting covariates are listed in Table 7.

To capture information about measurement patterns, cumulative missingness indicators were added as additional time-dependent covariates. Static covariates include sex, age, height, and weight at admission.

The final dataset contains 3,556 patients. We use 80% of the data for training and 20% for testing, with the training set further split into 80% training and 20% validation data.

Data availability: The public MIMIC-IV dataset (Johnson et al., 2023; Goldberger et al., 2000) is available under <https://physionet.org/content/mimiciv/2.2/> and is shared by the data owners after reasonable request.

A.4 Hyperparameter Tuning

A.4.1 Hyperparameter Tuning of ObsNODE

For hyperparameter optimization of the ObsNODE model, we use Optuna with the Tree-structured Parzen Estimator (TPE). Table 8 summarizes the search space (a) and the selected configurations for three datasets: the synthetic cancer dataset, the semi-synthetic MIMIC-IV dataset, and the MIMIC-IV sepsis dataset (b). While the parameters of the NODE component can, in principle, be tuned separately for each neural network in the observation normal form (5), we keep them identical across all components in our experiments.

VARIABLE	UNIT
SOFA SCORE	-
ALANINE AMINOTRANSFERASE	IU/L
ANION GAP	MEQ/L
BICARBONATE	MEQ/L
TOTAL BILIRUBIN	MG/DL
BLOOD UREA NITROGEN (BUN)	MG/DL
CREATININE	MG/DL
DIASTOLIC BLOOD PRESSURE	MMHG
PLATELET COUNT	K/ μ L
RED CELL DISTRIBUTION WIDTH (RDW)	%
SYSTOLIC BLOOD PRESSURE	MMHG

Table 7: Time-dependent covariates from MIMIC-IV-sepsis dataset

SEARCH SPACE/DATA SET	SYNTHETIC CANCER	(SEMI-SYNTHETIC) MIMIC-IV
LATENT SPACE DIMENSION	$[d_y, \dots, d_y * 3]$	$[d_y, \dots, d_y * 3]$
BATCH SIZE	$\{32, 64, \dots, 256\}$	$[100, 250, 500, 750, 1000]$
LEARNING RATE	$[0.001, 0.0001, 0.00001]$	$[0.001, 0.0001, 0.00001]$
HIDDEN DIM OBSERVER	$[32, 64, 128, 256]$	$[32, 64, 128, 256]$
HIDDEN DIMENSION NODE	$[32, 64, 128, 256]$	$[32, 64, 128, 256]$
NUMBER OF LAYERS NODE	$\{1, 2, \dots, 10\}$	$\{1, 2, \dots, 10\}$
ACTIVATION FUNCTION NODE	[LEAKYRELU, TANH, SIGMOID]	[LEAKYRELU, TANH, SIGMOID]

(a) Search space for ObsNODE hyperparameters.

HYPERPARAMETER/DATA SET	SYNTHETIC CANCER	SEMI-SYNTHETIC MIMIC-IV	MIMIC-IV
LATENT SPACE DIMENSION = $d_y \times m$	2×2	1×2	11×3
BATCH SIZE	64	100	500
LEARNING RATE	0.001	0.0001	0.0001
HIDDEN DIMENSION OBSERVER	128	128	256
HIDDEN DIMENSION NODE	128	128	256
NUMBER OF LAYERS NODE	5	6	7
ACTIVATION FUNCTION NODE	LEAKYRELU	LEAKYRELU	LEAKYRELU

(b) Optimized hyperparameter values for ObsNODE.

Table 8: **Hyperparameter Tuning of the ObsNODE Model.** Table (a) illustrates the hyperparameter search space, while Table (b) reports the optimal hyperparameter configurations for experiments conducted on the synthetic cancer dataset, the semi-synthetic MIMIC-IV sepsis dataset, and the MIMIC-IV sepsis dataset.

A.4.2 Hyperparameter Tuning of OptAB and DoseAI

For hyperparameter tuning of the OptAB and DoseAI models, we use Optuna with the Tree-structured Parzen Estimator (TPE). Table 9 summarizes the search space (a) and the resulting configurations (b) for both models. DoseAI can handle continuous treatment doses and is applied to the synthetic cancer dataset, while OptAB is restricted to categorical treatments and used for the semi-synthetic dataset based on MIMIC-IV and the real world sepsis dataset from MIMIC-IV. The decoder optimization is initialized with the final hyperparameter values obtained for the encoder.

SEARCH SPACE/DATA SET	SYNTHETIC CANCER	(SEMI-SYNTHETIC) MIMIC-IV
DIMENSION OF THE LATENT STATE	{1, 2, ..., 30}	{1, 2, ..., 30}
BATCH SIZE	{16, 32, 64, 125, 250, 500, 1000}	{100, 200, 500, 1000, 2000}
MAX. NUMBER OF NCDE UNITS	{1, 2, ..., 1000}	{1, 2, ..., 1000}
LEARNING RATE	[0.0001, 0.01]	[0.0001, 0.01]
ACTIVATION FUNCTION OF F	{LEAKYRELU, TANH, SIGMOID, IDENTITY}	{LEAKYRELU, TANH, SIGMOID, IDENTITY}
NUMBER OF NCDE LAYERS	{1, 2, ..., 20}	{1, 2, ..., 20}
ACTIVATION FUNCTION OF h_α	{LEAKYRELU, TANH, SIGMOID, IDENTITY}	{LEAKYRELU, TANH, SIGMOID, IDENTITY}
NUMBER OF LAYERS OF H	{1, 2, ..., 1000}	{1, 2, ..., 1000}
MAX. NUMBER OF UNITS OF H	{1, 2, ..., 6}	{1, 2, ..., 6}

(a) Search space for OptAB and DoseAI hyperparameters.

HYPERPARAMETER/DATA SET	SYNTHETIC CANCER	SEMI-SYNTHETIC MIMIC-IV	MIMIC-IV
ENCODER			
DIMENSION OF THE LATENT STATE	16	7	17
BATCH SIZE	250	1000	500
MAX. NUMBER OF NCDE UNITS	578	174	33
LEARNING RATE	0.0042	0.0016	0.0051
ACTIVATION FUNCTION OF F	LEAKYRELU	LEAKYRELU	TANH
NUMBER OF NCDE LAYERS	2	14	15
ACTIVATION FUNCTION OF h_α	TANH	LEAKYRELU	TANH
NUMBER OF LAYERS OF H	128	275	128
MAX. NUMBER OF UNITS OF H	4	4	1
DECODER			
DIMENSION OF THE LATENT STATE	22	25	17
BATCH SIZE	125	1000	1000
MAX. NUMBER OF NCDE UNITS	802	825	33
LEARNING RATE	0.0016	0.0007	0.0051
ACTIVATION FUNCTION OF F	LEAKYRELU	IDENTITY	TANH
NUMBER OF NCDE LAYERS	13	9	15
ACTIVATION FUNCTION OF h_α	LEAKYRELU	LEAKYRELU	TANH
NUMBER OF LAYERS OF H	798	403	128
MAX. NUMBER OF UNITS OF H	1	1	1

(b) Optimized hyperparameter values for OptAB and DoseAI Models.

Table 9: **Hyperparameter Tuning of the OptAB and DoseAI Models.** Table (a) presents the hyperparameter search space, while Table (b) reports the optimal hyperparameter configurations. DoseAI is used for training on the synthetic cancer dataset, whereas OptAB is applied to the semi-synthetic data set and the real world sepsis dataset from MIMIC-IV.

A.4.3 Hyperparameter Tuning of IGC-Net

For hyperparameter tuning of the IGC-Net model, we employ the Hydra implementation of the random grid search strategy for computational efficiency reasons. Table 8 presents the hyperparameter search space (a) and the selected hyperparameter configuration (b) of the IGC-Net model.

SEARCH SPACE/ DATA SET	SYNTHETIC CANCER	SEMI-SYNTHETIC MIMIC-IV	MIMIC-IV
TRANSFORMER BLOCKS	[1,2]	1	1
LEARNING RATE (η)	[0.01, 0.001, 0.0001]	[0.001, 0.0001, 0.0001]	[0.001, 0.0001]
MINIBATCH SIZE	[64, 128, 256]	[32,64,128, 256,512]	[32,64]
ATTENTION HEADS	1	[1,2,3]	[2,3]
TRANSFORMER UNITS	$[1d_g, 2d_g,$ $3d_g, 4d_g]$	$[1d_g, 2d_g,$ $3d_g, 4d_g]$	$[0.5d_g, 1d_g]$
HIDDEN REPRESENTATION SIZE	$[0.5d_g, 1d_g,$ $2d_g, 3d_g, 4d_g]$	$[1d_g, 2d_g,$ $3d_g, 4d_g]$	$[0.5d_g, 1d_g,$ $2d_g]$
FEED-FORWARD HIDDEN UNITS	$[0.5d_z, 1d_z,$ $2d_z, 3d_z, 4d_z]$	$[1d_z, 2d_z,$ $3d_z, 4d_z]$	$[0.5d_z, 1d_z,$ $2d_z]$
SEQUENTIAL DROPOUT RATE	[0.1, 0.2]	[0.1, 0.2]	[0.1, 0.2]
MAX POSITIONAL ENCODING	15	30	15
NUMBER OF EPOCHS	50	100	100

(a) Search space for IGC-Net hyperparameters.

HYPERPARAMETER/DATA SET	SYNTHETIC CANCER	SEMI-SYNTHETIC MIMIC-IV	MIMIC-IV
TRANSFORMER BLOCKS	2	2	1
LEARNING RATE	0.01	0.01	0.001
MINIBATCH SIZE	64	64	64
ATTENTION HEADS	0.1	1	2
TRANSFORMER UNITS	32	24	30
HIDDEN REPRESENTATION SIZE	64	72	30
FEED-FORWARD HIDDEN UNITS	32	18	30
SEQUENTIAL DROPOUT RATE	0.1	0.1	0.1
MAX POSITIONAL ENCODING	15	30	15
NUMBER OF EPOCHS	50	100	100

(b) Optimized hyperparameter values for IGC-Net.

Table 10: **Hyperparameter Tuning of the IGC-Net Model.** Table (a) presents the hyperparameter search space, while Table (b) reports the optimal hyperparameter configurations of the IGC-Net model for experiments conducted on the synthetic cancer dataset, the semi-synthetic MIMIC-IV dataset, and the real world MIMIC-IV sepsis dataset. The overall input dimension is given by $d_g = d_y + d_x + d_a$, and d_z denotes the hidden representation size of the IGC-Net model.

A.4.4 Hyperparameter Tuning of SCIP-Net

For hyperparameter tuning of the SCIP-Net model for the synthetic cancer data and semi-synthetic data, we employed the Hydra–Optuna implementation of the Tree-structured Parzen Estimator (TPE). For the real sepsis data, we tuned the SCIP-Net model using a random grid search. Hyperparameter optimization with Optuna using the Tree-structured Parzen Estimator (TPE) did not yield improved or optimal parameter configurations.

Table 11c summarizes the hyperparameter search space (a) and the selected configurations (b) for the synthetic cancer dataset, the semi-synthetic MIMIC-IV sepsis dataset, and the MIMIC-IV sepsis dataset.

A.5 Computational efficiency

For training and hyperparameter optimization of ObsNODE we utilized two Nvidia A100 GPUs, each with 40 GB of memory. The same setting was used for the baseline models DoseAI, OptAB and SCIP-Net. For ICG-Net, we used a NVIDIA H100 GPU with 96 GB of memory.

SEARCH SPACE MODEL	WEIGHT NETWORK, TREATMENT NETWORK, ENCODER	DECODER
NEURAL CDE HIDDEN LAYERS	[1,2]	[1,2]
LEARNING RATE	[0.01,0.001, 0.0001, 0.0001]	[0.01,0.001, 0.0001, 0.0001]
MINIBATCH SIZE	[64,128,256]	[256,512,1024]
NEURAL CDE HIDDEN UNITS	[0.5,1,2,3,4] d_g	[1,2,3,4,8,16] d_g
NEURAL CDE DROPOUT RATE	[0.1,0.2]	[0.1,0.2]
MAX. GRADIENT NORM	[0.5,1,2]	[0.5,1.0,2.0,4.0]
EPOCHS	50	50

(a) Search space for SCIP-Net hyperparameters.

PARAMETER / MODEL	WEIGHT NETWORK	TREATMENT NETWORK	ENCODER	DECODER
SYNTHETIC CANCER				
NEURAL CDE HIDDEN LAYERS	2	1	1	2
LEARNING RATE	0.0001	0.01	0.01	0.001
MINIBATCH SIZE	128	64	64	256
NEURAL CDE HIDDEN UNITS	8	12	8	32
NEURAL CDE DROPOUT RATE	0.1	0.1	0.1	0.1
MAX. GRADIENT NORM	0.5	0.5	0.5	1
SEMI-SYNTHETIC MIMIC-IV				
NEURAL CDE HIDDEN LAYERS	1	2	2	2
LEARNING RATE	0.01	0.01	0.01	0.0001
MINIBATCH SIZE	64	64	256	256
NEURAL CDE HIDDEN UNITS	9	12	6	12
NEURAL CDE DROPOUT RATE	0.1	0.1	0.2	0.2
MAX. GRADIENT NORM	0.5	0.5	2	1
MIMIC-IV				
NEURAL CDE HIDDEN LAYERS	2	2	1	2
LEARNING RATE	0.01	0.01	0.01	0.01
MINIBATCH SIZE	256	256	256	512
NEURAL CDE HIDDEN UNITS	42	42	42	84
NEURAL CDE DROPOUT RATE	0.2	0.1	0.1	0.1
MAX. GRADIENT NORM	0.5	2.0	2.0	0.5

(b) Optimized hyperparameter values for SCIP-Net.

(c) **Hyperparameter Tuning of the SCIP-Net Model.** Table (a) presents the hyperparameter search space. Table (b) reports the optimal configurations for the synthetic cancer dataset and the semi-synthetic MIMIC-IV sepsis dataset and the real world MIMIC-IV sepsis dataset.

Training of ObsNODE for the optimal hyperparameter values on a single Nvidia A100 GPU took 140 min for the synthetic cancer data, 49 min for the semi-synthetic data and 65 min for the real world sepsis data.

This is similar to the training times required for the baseline models ICG-Net and SCIP-Net. Training OptAB and DoseAI required between 40 and 74 hours, depending on the data set.

A.6 Declaration of LLM usage

The core method development in this research does not involve LLMs as any important original, or non-standard components.